Distance Protection Relaying in Distribution Grids with Increasing Inverter-Based-Resources

Jonathan Loebel*, Gregor Becker, Johann Jaeger
Friedrich-Alexander-Universität Erlangen-Nürnberg
Erlangen, Germany
*jonathan.loebel@fau.de

Kai Trunk, Johannes Leugner, Christian Scheibe
Siemens AG
Erlangen, Germany

***Abstract*—The number of renewable energy sources in distribution grids is increasing. Most of those plants are connected to the grid via inverters. Those inverter-based-resources (IBRs) are mainly controlled in grid-following mode (GFL). Prior research explained the influence of those GFL IBRs on distance protection, a widely spread grid protection algorithm. In this paper the prior findings are evaluated in a developing distribution grid. During four development stages, the number of GFL IBRs increases. Moreover, the GFL IBRs follow the three common fault-ride-trough (FRT) techniques. All relevant protection relays are analyzed for critical grid faults in each stage and each FRT. The results confirm the findings of the prior research. Active power in the positive sequence, reactive power in the positive sequence and reactive power in the negative sequence influence the measured impedance of the distance protection in different ways. In critical cases, this can lead to incorrect measurements. Additionally it is shown, that typical developments in distribution grids can impact the critical grid protection negatively. The test framework will in future serve for newly developed protection algorithms that address the problems described.**

***Index Terms*—Distribution Grid, Protection, Distance Protection, Inverter-Based-Resources**

I. Introduction

In Germany, over 95 % of the installed capacity of wind and PV plants was connected to the distribution grid in 2019 [1]. Those plants are mostly connected to the grid via inverters. As the number of those renewable energy sources (RES) is increasing rapidly, the impact of inverter-based-resources (IBRs) on the distribution grid grows. State-of-the-art of IBR control mode is grid-following (GFL) [2], [3]. The behavior of GFL IBRs differs fundamental to classical synchronous generators (SG), especially during grid faults [4]. In future, many IBR systems are planned in grid-forming (GFM) mode. In addition to these changes, the flow of power within the grid is changing due to the decentralized location of RES in contrast to centralized SG at higher voltage levels [5]. These changes lead to a different behavior of the electrical grid during grid faults. Regardless of these changes, the grid protection must work secure, reliable and dependable. The most widespread protection algorithms in distribution grids are the overcurrent and distance protection. This paper focuses on the distance protection algorithm. Previous research shows significant malfunction of this algorithm in the presence of GFL IBRs [6]–[9].

The authors gratefully acknowledge funding by the German Federal Ministry of Research, Technology and Space (BMFTR) within the Kopernikus Project ENSURE ‘New ENergy grid StructURes for the German Energiewende’.

Prior research explained the behavior of the distance protection algorithm under the influence of GFL IBRs [10]. A simple system is considered for an analytical explanation. A GFL IBR is connected to an external grid via a transmission line. A grid fault is applied to this line. The impact of active and reactive power in the positive sequence, as well as reactive power in the negative sequence are analytical explained. Therefore, the influence of the three typical fault-ride-trough (FRT) variants on the distance protection can be explained. The information is summarized briefly in II. The findings from the previous work are evaluated in this paper in a distribution grid. The basic structure as well as a detailed description of the components is shown in [11]. Four development stages are examined. The number of IBRs is steadily increasing as PV parks, wind farms, and batteries are connected to the grid. These correspond to the progression from a grid without converters to a modern grid permeated with renewable energies, which is representative for the characteristic development of typical distribution grids in Germany. A Grid fault is simulated at each stage and the affected distance protection relays are analyzed. The investigations will serve as a basis for the future analysis and evaluation of newly developed protection algorithms within the Kopernikus ENSURE project.

In III the four development stages of the considered distribution grid are introduced. In each stage, the number of IBRs increases. Therefore, GFL IBR control is explained. Moreover the protection scheme of the grid is presented. In IV grid fault analysis are shown for each stage for the three different FRT techniques. The reliability and dependability of the protection scheme is analyzed. In V the results are concluded and an outlook for further research is given.

II. Distance Protection under the Influence of GFL IBR

[10] provides an analytical representation of how GFL IBR control affects distance protection during FRT in the event of a two-phase grid fault. The feed-in of active power in the positive sequence, reactive power in the positive sequence, and reactive power in the negative sequence are considered individually. A simple grid is considered, consisting of a

979-8-3315-8138-1

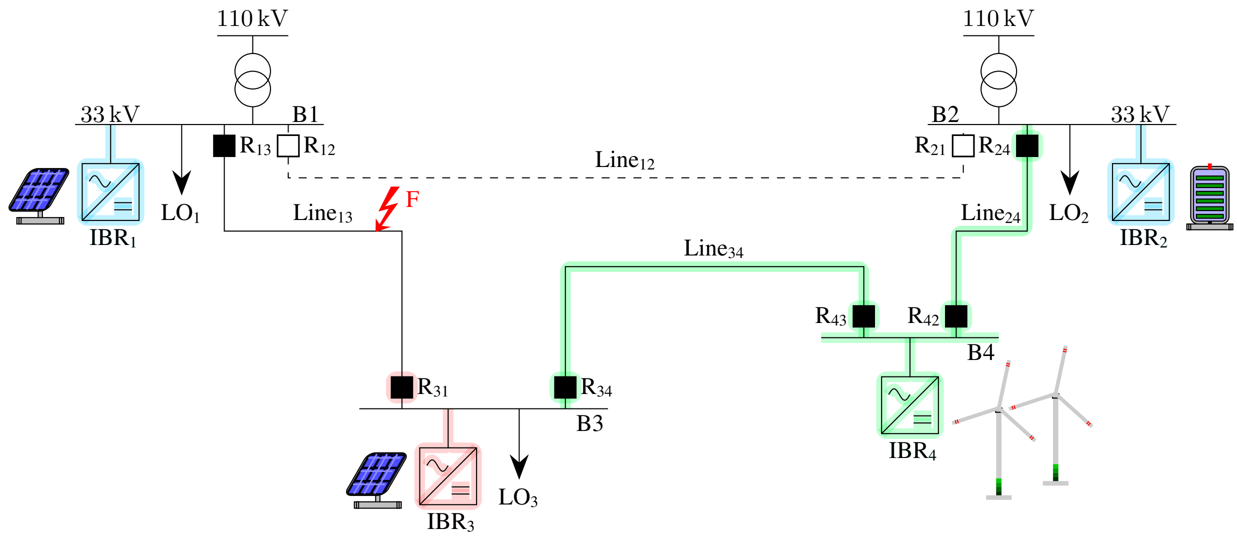

Fig. 1: Structure of considered distribution grid during development stages 1 (black), 2 (red), 3 (green) and 4 (blue) with increasing number of IBRs.

GFL IBR connected to an external grid via a transmission line. A fault on this line is considered from the perspective of the protection device on the IBR side. Fig. 2 shows this influence. It is based on (1). The measured impedance is composed of the affected line impedance $m\underline{Z}_\mathrm{L}$ and the measurement error. The latter consists of the fault resistance R_F as fixed value, as well as a current factor to the fault resistance as variable. This depends on the IBR phase currents and grid phase currents. The magnitude of this part cannot be influenced, as the short-circuit current level of the external grid and the GFL IBR are considered fixed. However, the angle can be influenced by the FRT control of the GFL IBR. If this is minimal, the deviation of the measured distance is also minimal, as only the reactance is used for location.

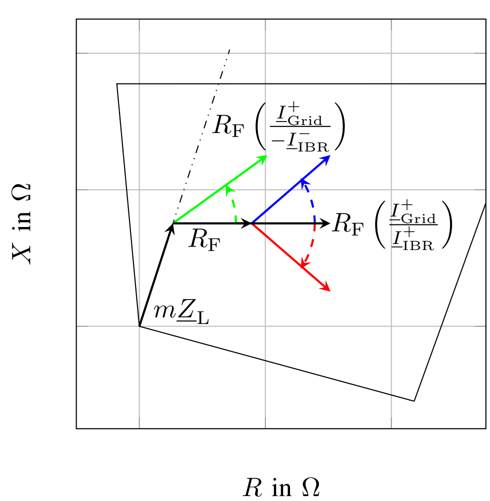

Fig. 2: Influence of active (red) and reactive (blue) power in positive sequence and reactive power feed in negative sequence (green) on distance protection.

$$\underline{Z}_\mathrm{meas,bc} = m\underline{Z}_\mathrm{L} + \underbrace{\frac{R_\mathrm{F}}{2}\left(1 + \frac{\underline{I}_\mathrm{IBR,b} - \underline{I}_\mathrm{IBR,c}}{\underline{I}_\mathrm{Grid,b} - \underline{I}_\mathrm{Grid,c}}\right)}_{\text{measurement error}} \quad (1)$$

Active power feed in the positive sequence (red) leads to a clockwise rotation additional fault resistance factor. In contrast, reactive power feed in the positive sequence (blue) leads to a counterclockwise rotation. Reactive power feed in the negative sequence (green) hast the same effect as in the positive sequence, but with a different mathematical basis.

These findings are now evaluated on a larger, more complex electrical grid with multiple IBRs and changing grid structures.

III. Distribution Grid

A. Development Stages

Fig. 1 illustrates the considered 33 kV distribution grid, with all relevant parameters listed in Tab. I. The initial state (Stage 1) is depicted in black. Stations B1 and B2 are supplied by the overlaid 110 kV grid. A possible connection between both stations via Line_{12} remains open. Moreover, Station B3 is connected to B1 via Line_{13}. A constant load is connected to each station, with a power factor of $\cos\varphi = 0.9$. In Stage 2 (red), a PV park is connected to B3 via IBR_3. Therefore, protection relay R_{31} is added to switch off feeding of grid faults from bus B3. In Stage 3 (green), a new Station B4 is added to connect a large wind farm to B2 via Line_{24} and B3 via Line_{34}. The Wind park is represented by IBR_4. In Stage 4 (blue), a PV park is connected to B1 via IBR_1. Additionally, a large battery storage is connected to B2. All IBRs operate in GFL mode and follow the FRT techniques, explained in III-B.

The EMT simulation of the electrical grid is performed in PSS®NETOMAC. The GFL IBR models are simulated in MATLAB Simulink. Both programs are linked via a co-simulation interface [12].

979-8-3315-8138-1

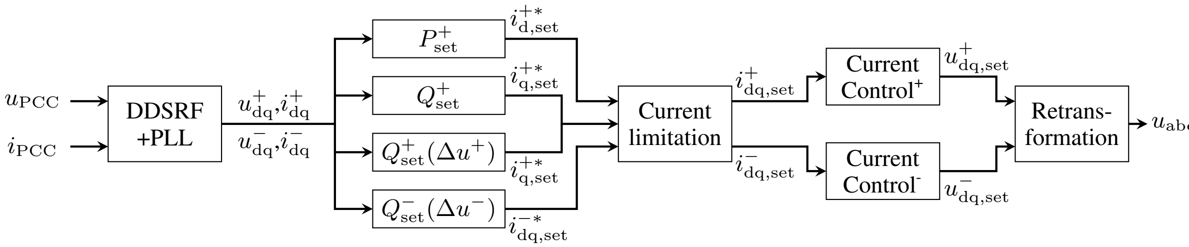

Fig. 3: Grid-Following control schemes for IBRs with normal operation and FRT statics in positive and negative sequence.

B. GFL IBR Control Scheme

The IBRs are connected to the grid via an LCL-Filter and a transformer. The GFL control scheme is illustrated simplified in Fig. 3, based on [13], [14]. First, a Decoupled Double Synchronous Reference Frame (DDSRF) is utilized to separate abc voltage and current values from the Point of Common Coupling (PCC), on the grid side of the transformer, into positive ($^+$) and negative ($^-$) sequence dq components. Synchronization with the grid is achieved by a Phase-Locked Loop (PLL) that controls u^+_{q} to zero. During normal operation, active power (P^+_{set}) and reactive power (Q^-_{set}) define the set values i^+_{d} and i^+_{q}, respectively. The negative sequence set points are set to zero. During grid faults the control can follow three different modes. First, only active power is supplied. Therefore, $i^+_{\mathrm{q,set}}$ and $i^-_{\mathrm{dq,set}}$ are set to zero. Secondly, active and reactive power in the positive sequence are fed. Reactive power is defined using a static calculation based on the voltage deviation, as shown in (2).

$$Q^{+/-}_{\mathrm{set}} = k^{+/-} \cdot \Delta u^{+/-} \tag{2}$$

The negative sequence current $i^-_{\mathrm{dq,set}}$ is still set to zero. In current limiting, $i^+_{\mathrm{q,set}}$ has a higher priority than $i^+_{\mathrm{d,set}}$. That means that $i^+_{\mathrm{d,set}}$ is reduced if necessary in order to reach the set point of $i^+_{\mathrm{q,set}}$. This is based on the voltage-supporting behavior of reactive power during FRT. Third, active and reactive power in the positive sequence, as well as reactive power in the negative sequence are fed. The negative sequence reactive power is also calculated following (2). Its purpose is to provide symmetry in the event of asymmetrical grid conditions caused by grid faults. In this case an unsymmetrical current limitation is applied to limit the set point [15], [16]. Reactive currents are given higher priority than active currents, while the reactive currents of the positive and negative sequences have equal priority. These three FRT techniques cover a large number of common grid codes [7]. The limited current set points are controlled by two separate current controls for the positive and negative sequences. The re-transformation converts $u^{+/-}_{\mathrm{dq}}$ values to abc values, which are then given into controlled voltage sources.

TABLE I: Grid parameters for four development stages.

	Stage 1	Stage 2	Stage 3	Stage 4
S_{LO1}	4 MVA	4 MVA	6 MVA	7 MVA
S_{LO2}	10 MVA	12 MVA	14 MVA	16 MVA
S_{LO3}	1 MVA	1 MVA	3 MVA	4 MVA
S_{IBR1}	-	-	-	5 MVA
S_{IBR2}	-	-	-	20 MVA
S_{IBR3}	-	8 MVA	8 MVA	8 MVA
S_{IBR4}	-	-	16 MVA	16 MVA
l_{Line}	4 km			
R'_{Line}	0.061 Ω			
X'_{Line}	0.173 Ω			

C. Grid Protection

This paper focuses on directed polygon distance protection. A distance protection scheme is applied, based on [17]–[19]. Relays R_{13}, R_{34}, R_{24} and R_{43} operate with three protection zones, while R_{42} and R_{31} operate with two protection zones, as a third zone does not protect the considered lines. In Stage 1 only relay R_{13} is considered. As a fault on Line_{13} is fed from both sides in Stage 2, a second relay R_{31} is added at B3. As B4 is added in Stage 3 with Line_{34} and Line_{24}, relays R_{34}, R_{43}, R_{24} and R_{42} are added to protect the lines. Fig. 4 shows the connected lines and relays with protection zones. Each section of the line is thus protected at least doubly. The primary protection zone Z1 is calculated by (3). The secondary protection zone Z2 is used as backup for the next protection relay zone and calculated by (4). The tertiary protection zone Z3 is calculated by (5).

$$\underline{Z}_{\mathrm{Z1}} = 0.9\underline{Z}_{\mathrm{Line1}} + \frac{R_{\mathrm{A}}}{2} \tag{3}$$

$$\underline{Z}_{\mathrm{Z2}} = 0.9\left(\underline{Z}_{\mathrm{Line1}} + 0.85\underline{Z}_{\mathrm{Line2}}\right) + \frac{R_{\mathrm{A}}}{2} \tag{4}$$

$$\underline{Z}_{\mathrm{Z3}} = 0.9\left(\underline{Z}_{\mathrm{Line1}} + 0.85\left(\underline{Z}_{\mathrm{Line2}} + 0.85\underline{Z}_{\mathrm{Line3}}\right)\right) + \frac{R_{\mathrm{A}}}{2} \tag{5}$$

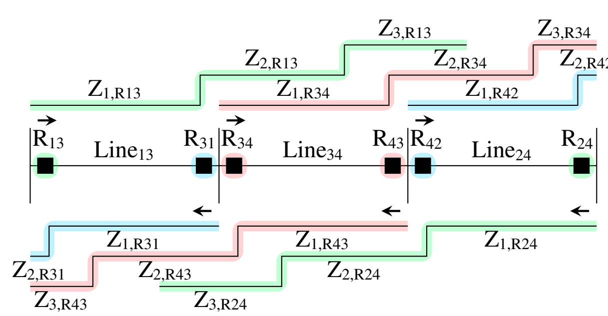

Fig. 4: Distance protection scheme for considered distribution grid with primary and backup protection zones.

979-8-3315-8138-1

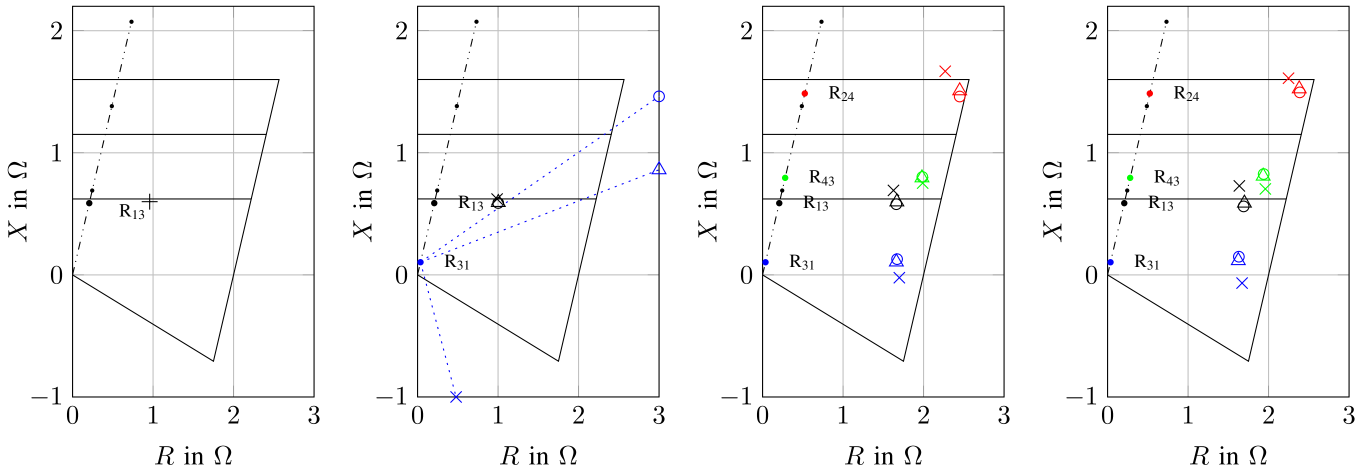

(a) (b) (c) (d)

Fig. 5: Distance Protection measurements during fault F1 at Stage 1 (a), Stage 2 (b), Stage 3 (c) and Stage 4 (d) with different FRT techniques: P^{+}(x), P^{+} and Q^{+}(o), P^{+}, Q^{+} and Q^{-} (Δ).

The arc compensation $\frac{R_A}{2}$ is set to $2\,\Omega$. This value is oriented on typical arc resistances in medium voltage grids [20]. Overcurrent time protection is not used as a backup in the simulation, as the focus is on distance protection.

IV. Distance Protection Analysis

First, a two-phase-fault F with a fault resistance of $1.5\,\Omega$ at 85 % of Line_{13} is simulated. Fig. 5 shows the relevant section of the distance protection measurements during the four stages. The dash-dotted line represents the three consecutive lines with a black dot at the end of each. The three protection zones are illustrated. The measured impedances for the different FRT techniques are marked with “x” for pure active power feed, “o” for additional reactive power feed in the positive sequence and “Δ” for additional reactive power feed in the negative sequence.

In Stage 1, only relay R_{13} protects Line_{13}. In Fig. 5a a black dot represents the line impedance from the relay to the fault. It is close to the zone boundary, which makes it critical for correct measurement. The ”+” marks the actual measured impedance by the relay during the grid fault. As expected, the measured impedance is shifted by half the fault resistance in the positive R direction. Due to sufficient fault resistance compensation, the fault is correctly localized in zone Z1.

In Stage 2, relay R_{13} and R_{31} protect Line_{13}. In Fig. 5b the black dot represents the line impedance from the relay to the fault for relay R_{13}, while the blue dot represents it for relay R_{31}. Independent of the FRT technique of the GFL IBR, relay R_{13} detects the fault correctly in zone Z1. The short-circuit current of the GFL IBR is very small compared to that of the external grid. Therefore, the effects described in II are hardly visible. However, a closer look at the values reveals that the measured impedance shifts in positive X direction during pure active power is feed. Therefore, the measured impedance is almost at the zone boundary. When reactive power is fed into the positive or positive and negative sequence, a shift in the negative X direction can be seen. Relay R_{31} does not detect the fault, independent of the FRT technique. The measured values are far outside the range shown. The direction is indicated by the dotted blue line and the symbols. Using (1), the effect is due to the small GFL IBR currents, compared to the external grid. An active power feed in the positive sequence leads to a clockwise rotation of the measured impedance. A reactive power feed in the positive sequence leads to a counterclockwise rotation. If the reactive power static in the positive sequence is activated, in Stage 2 IBR_3 purely feeds reactive power, due to the large voltage drop. Reactive power feed in the negative sequence also leads to a counterclockwise rotation. Still, due to effects of a changed network the angle deviation is less then in the positive sequence. The measurements correspond to the effect described in II. The opposite applies to Relay R_{13}, which can be explained by the opposite direction of both relays.

In Stage 3 the grid structure changes fundamentally. Now the fault F should be detected by four protection relays. R_{13} and R_{31} serve as primary protection, while R_{43} and R_{24} are backup protection. In Fig. 5c the colored dots mark the line impedance from the relay to the fault for R_{13} in black, R_{31} in blue, R_{43} in green and R_{24} in red. Now, the length of all measurement deviation is in the same range for all relays. This is because the overlaid external grid is now connected via stations B1 and B2 and feeds into the fault from both sides. Accordingly, the current amplitudes are in a similar range. Still the described effect can be seen. Relays R_{31} and R_{43} are located next to buses fed by IBRs. Therefore the effect is as described before, still, with less influence due to the short circuit current of the external grid. Both relays detect the fault in the correct protection zones, independent of the FRT technique. Relays R_{13} and Relay R_{24} are located on buses opposite of buses with IBRs. Therefore, like described for R_{13} in Stage 2, the effect is contrary. This can clearly be seen and

979-8-3315-8138-1

leads to malfunction during pure active power feed during FRT. Relay R_{13} locates the fault in zone Z2 instead of Z1. Relay R_{24} does not detect the fault anymore, as the measured reactance overreaches Z3. Still for both other FRT techniques, the relays locate the fault correctly.

In Stage 4 GFL IBRs are added to the buses B1 and B2. The marks in Fig. 5d correspond to those before. As now both sides of $Line_{24}$ are fed by GFL IBRs, the described effects decrease at relay R_{24}. Still for pure active power feed by the IBRs during FRT, the relay does not detect the fault. At relay R_{43} and R_{31} the effect increases due to the feed of GFL IBRs at the opposite buses. Still both relays detect the fault correctly in zone Z2 and Z1, respectively. For relay R_{13} the effect increases. Therefore, with pure active power feed by the IBRs during FRT, the fault is wrongly detected in zone Z2 instead of Z1. For both other FRT techniques, the fault is correctly detected in Z1.

V. Conclusion and Outlook

The studies show that the previous investigations also apply in a larger, more complex electrical grids. If the fault fed on both sides is fed on one side not only by a GFL IBR but also by an external grid, the effect is weakened but still clearly noticeable. In critical cases, such as grid faults near the zone boundary of the distance protection, the FRT control of the GFL IBR can lead to incorrect fault location. Feeding reactive power into the positive sequence or positive and negative sequence leads to significantly better results than feeding in active power alone.

The different stages of the distribution grid show, that the grid protection can clearly be affected by an increasing number of GFL IBRs. Therefore, such developments must be taken into account in terms of grid protection. Both the necessary changes in the structure and the control behavior of the IBRs play an important role here.

The results and the framework presented will be used for further research in the field of grid protection in the future. The IBRs will be expanded to include GFM mode. While GFL mode is currently the most widely used control mode, IBRs will in future be operated in GFM mode. In addition, novel protection algorithms will be tested in the framework to eliminate the problems identified.

References

[1] Bundesnetzagentur, "Eeg in zahlen [eeg in figures]," Bundesnetzagentur, Tech. Rep., 2019, stand: 19 Apr 2021. [Online]. Available: https://www.bundesnetzagentur.de/DE/Fachthemen/ElektrizitaetundGas/ErneuerbareEnergien/EE-Statistik/start.html

[2] Y. Lin, J. H. Eto, B. B. Johnson, J. D. Flicker, R. H. Lasseter, H. N. V. Pico, G.-S. Seo, B. J. Pierre, and A. Ellis, "Research roadmap on grid-forming inverters," no. NREL/TP-5D00-73476, 2020. [Online]. Available: https://www.nrel.gov/docs/fy21osti/73476.pdf

[3] B. Kroposki, B. Johnson, Y. Zhang, V. Gevorgian, P. Denholm, B.-M. Hodge, and B. Hannegan, "Achieving a 100% renewable grid: Operating electric power systems with extremely high levels of variable renewable energy," *IEEE Power and Energy Magazine*, vol. 15, no. 2, pp. 61–73, Mar. 2017. [Online]. Available: http://ieeexplore.ieee.org/document/7866938/

[4] C. Mozina, "Impact of green power inverter-based distributed generation on distribution systems," in *2014 67th Annual Conference for Protective Relay Engineers*, 2014, pp. 264–278.

[5] T. Keil, *Schutzsysteme für elektrische Energieversorgungsnetze mit dezentralen Stromerzeugungsanlagen*, ser. Berichte aus der Elektrotechnik. Aachen, Germany: Shaker Verlag, 2011.

[6] A. Hooshyar, M. A. Azzouz, and E. F. El-Saadany, "Distance protection of lines emanating from full-scale converter-interfaced renewable energy power plants—part i: Problem statement," *IEEE Transactions on Power Delivery*, vol. 30, no. 4, pp. 1770–1780, 2015.

[7] M. Kleemann and N. Baeckeland, "Converter meets distance protection: A good match?" in *2021 23rd European Conference on Power Electronics and Applications (EPE'21 ECCE Europe)*, 2021, pp. 1–10.

[8] J. Jia, G. Yang, A. H. Nielsen, and P. Rønne-Hansen, "Impact of vsc control strategies and incorporation of synchronous condensers on distance protection under unbalanced faults," *IEEE Transactions on Industrial Electronics*, vol. 66, no. 2, pp. 1108–1118, 2019.

[9] A. Novikov, J. J. de Chavez, and M. Popov, "Performance assessment of distance protection in systems with high penetration of pvs," in *2019 IEEE Milan PowerTech*, 2019, pp. 1–6.

[10] J. Loebel, A. Kuri, T. R. Bermudez *et al.*, "Distance protection relaying under the impact of grid-following inverter-based-resources," *TechRxiv*, Nov. 2025, preprint.

[11] J. Leugner, J. Loebel, K. Trunk, D. Da Cruz, and C. Scheibe, "A modular and flexible power system test grid for stability and protection analysis of converter-dominated grids," in *ETG Kongress 2025; Voller Energie – heute und morgen.*, 2025, pp. 444–450.

[12] C. P. Scheibe, *Co-Simulation elektrischer Energiesysteme mit kommerziellen Programmsystemen: Architektur, Methodik und Anwendungen*, ser. FAU Studien aus der Elektrotechnik, Band 29. Erlangen: FAU University Press, 2025.

[13] R. Teodorescu, M. Liserre, and P. Rodríguez, *Grid Converters for Photovoltaic and Wind Power Systems*, 1st ed. Wiley, 2011.

[14] F. Mahr, S. Henninger, M. Biller, and J. Jaeger, *Electrical energy systems: knowledge networking of power converters, grid operation and grid protection, (in German)*. Wiesbaden: Springer Fachmedien, 2021.

[15] C.-T. Lee, C.-W. Hsu, and P.-T. Cheng, "A low-voltage ride-through technique for grid-connected converters of distributed energy resources," *IEEE Transactions on Industry Applications*, vol. 47, no. 4, pp. 1821–1832, 2011.

[16] T. Wijnhoven, G. Deconinck, T. Neumann, and I. Erlich, "Control aspects of the dynamic negative sequence current injection of type 4 wind turbines," in *2014 IEEE PES General Meeting — Conference & Exposition*, 2014, pp. 1–5.

[17] G. Ziegler, *Numerical Distance Protection: Principles and Applications*, 4th ed. Erlangen: Publicis Corporate Publishing, Siemens AG, 2011.

[18] S. H. Horowitz and A. G. Phadke, *Power System Relaying*, 3rd ed. Chichester, England, Hoboken, NJ: Wiley, 2008.

[19] C. R. Mason, *The Art and Science of Protective Relaying*. New York: Wiley, 1956.

[20] *Guide to the implementation of protection systems in electrical grids, (in German)*, VDE (FNN), Berlin, 2009.